Anal. Chem. **2002,** *74,* 3984−3990

A Microfabrication-Based Dynamic Array Cytometer

Joel Voldman,* Martha L. Gray,† Mehmet Toner,‡ and Martin A. Schmidt

Department of Electrical Engineering and Computer Science and Division of Health Sciences and Technology, Massachusetts Institute of Technology, Cambridge, Massachusetts 02139, and Center for Engineering in Medicine, Massachusetts General Hospital, Boston, Massachusetts 02114

We have developed a microfabricated device for use in parallel luminescent single-cell assays that can sort populations upon the basis of dynamic functional responses to stimuli. This device is composed of a regular array of noncontact single-cell traps. These traps use dielectrophoresis to stably confine cells and hold them against disrupting fluid flows. Using quantitative modeling, we have designed traps with a novel asymmetric extruded-quadrupole geometry. This new trap can be physically arrayed and electrically addressed, enabling our cytometer. Situating an array of these traps in a microchannel, we have introduced cells into the array and demonstrated observation of fluorescent dynamic responses followed by sorting. Such a device has potential for use in investigating functional processes, as revealed by temporal behavior, in large numbers of single cells.

As we enter the post-genome era, we undertake the task of translating genotype into phenotype. Microarray experiments, allowing for genome-wide analysis of transcriptional phenotypes, provide great insight into the workings of the cell.[1−3] The need also exists, however, to explore more complex *functional* phenotypes in order to fully understand cellular processes.

Dynamical processes in living cells are one set of complex phenotypes. Cells are inherently dynamical systems, with responses to intracellular and extracellular inputs that vary over time scales from less than seconds[4−6] to days.[1,7,8] Probing these dynamics can elucidate the signaling cascades and decision processes occurring within cells,[9−11] how time variations in signals can convey information,[12] and the dynamics underlying gene expression.[13,14]

Performing such assays on multiple single living cells gives several unique advantages. First, parallel analysis of living single cells can uncover individual phenotypic variations that would be masked in population assays while also capturing statistical variations within the population. Second, continuous monitoring of dynamics in living cells can capture information that might be missed as a result of undersampling in conventional timepoint experiments. In addition, single-cell analysis is well-suited for luminescent assays, taking advantage of the continuous introduction of new probes for cellular function, such as quantum dots,[15] fluorescence resonance energy transfer (FRET),[16] and fluorescent proteins.[17,18] Finally, the ability to sort living cells after performing dynamic analyses enables high-throughput subsequent isolation of cells based upon complex functional responses to stimulus. This allows for the efficient isolation of positively responding cells, easing investigation into the genomic or transcriptional profiles responsible for the dynamic behavior.

Current approaches to probing luminescent dynamic responses of populations of single cells using luminescent assays include microscopy,[19] flow cytometry,[20] and laser scanning cytometry.[21] Microscopy enables the researcher to study intracellular dynamics of a small population of cells but does not allow for subsequent sorting. Automated microscopy techniques, such as laser scanning cytometry and high-content screening,[22] remove the population limitations of conventional microscopy but still do not enable viable

* Corresponding author. E-mail: voldman@mit.edu.

† Division of Health Sciences and Technology, Massachusetts Institute of Technology.

‡ Massachusetts General Hospital.

(1) Iyer, V. R.; Eisen, M. B.; Ross, D. T.; Schuler, G.; Moore, T.; Lee, J. C. F.; Trent, J. M.; Staudt, L. M.; Hudson, J.; Boguski, M. S.; Lashkari, D.; Shalon, D.; Botstein, D.; Brown, P. O. *Science* **1999**, *283*, 83−87.

(2) Hughes, T. R.; Mao, M.; Jones, A. R.; Burchard, J.; Marton, M. J.; Shannon, K. W.; Lefkowitz, S. M.; Ziman, M.; Schelter, J. M.; Meyer, M. R.; Kobayashi, S.; Davis, C.; Dai, H.; He, Y. D.; Stephaniants, S. B.; Cavet, G.; Walker, W. L.; West, A.; Coffey, E.; Shoemaker, D. D.; Stoughton, R.; Blanchard, A. P.; Friend, S. H.; Linsley, P. S. *Nat. Biotechnol.* **2001**, *19*, 342−347.

(3) DeRisi, J. L.; Iyer, V. R.; Brown, P. O. *Science* **1997**, *278*, 680−686.

(4) Iino, M. *Mol. Cell Biochem.* **1999**, *190*, 185−190.

(5) Berridge, M. J. *Nature* **1993**, *361*, 315−325.

(6) Cheng, H.; Lederer, W. J.; Cannell, M. B. *Science* **1993**, *262*, 740−744.

(7) Cheng, T.; Shen, H.; Giokas, D.; Gere, J.; Tenen, D. G.; Scadden, D. T. *Proc. Natl. Acad. Sci. U.S.A.* **1996**, *93*, 13158−13163.

(8) Wen, X.; Fuhrman, S.; Michaels, G. S.; Carr, D. B.; Smith, S.; Barker, J. L.; Somogyi, R. *PNAS* **1998**, *95*, 334−339.

(9) McAdams, H. H.; Arkin, A. *Curr. Biol.* **2000**, *10*, R318−R320.

(10) Endy, D.; Brent, R. *Nature* **2001**, *409*, 391−395.

(11) Ideker, T.; Galitski, T.; Hood, L. *Ann. Rev. Genomics Hum. Genet.* **2001**, *2*, 343−372.

(12) Marshall, C. J. *Cell* **1995**, *80*, 179−185.

(13) Reis, B. Y.; Butte, A. S.; Kohane, I. S. *J. Biomed. Inform.* **2001**, *34*, 15−27.

(14) Holter, N. S.; Maritan, A.; Cieplak, M.; Fedoroff, N. V.; Banavar, J. R. *Proc. Natl. Acad. Sci. U.S.A.* **2001**, *98*, 1693−1698.

(15) Bruchez, M.; Moronne, M.; Gin, P.; Weiss, S.; Alivisatos, A. P. *Science* **1998**, *281*, 2013−2016.

(16) Janetopoulos, C.; Jin, T.; Devreotes, P. *Science* **2001**, *291*, 2408−2411.

(17) Heikal, A. A.; Hess, S. T.; Baird, G. S.; Tsien, R. Y.; Webb, W. W. *Proc. Natl. Acad. Sc.i U.S.A.* **2000**, *97*, 11996−12001.

(18) Tsien, R. Y. *Ann. Rev. Biochem.* **1998**, *67*, 509−544.

(19) Zlokarnik, G.; Negulescu, P. A.; Knapp, T. E.; Mere, L.; Burres, N.; Feng, L. X.; Whitney, M.; Roemer, K.; Tsien, R. Y. *Science* **1998**, *279*, 84−88.

(20) Martin, J. C.; Swartzendruber, D. E. *Science* **1980**, *207*, 199−201.

(21) Darzynkiewicz, Z.; Bedner, E.; Li, X.; Gorczyca, W.; Melamed, M. R. *Exp. Cell Res.* **1999**, *249*, 1−12.

10.1021/ac0256235 CCC: $22.00
Published on Web 07/10/2002

sorting. Flow cytometry, including microfluidic versions,[23] can be used to sort quickly, but because of its intrinsic flowing nature, can only interrogate each cell once, limiting its use in dynamic assays.

The ideal instrument for probing such dynamics would allow parallel luminescent probing of ensembles of single cells and include an automated high-throughput method to viably isolate positively responding subpopulations. We have developed a microfabricated cytometer that has the potential to meet these requirements. This microfabrication-based dynamic array cytometer—μDAC—consists of a planar array of single-cell traps that can be loaded with cells, interrogated over time, and then individually sorted, where the sort variable is the dynamic response. This combination of microscopy and subsequent viable sorting enables us to more fully explore complex phenotypes.

These traps use dielectrophoresis[24,25] (DEP), the force on polarization charges in a nonuniform electric field, to create strongly confining potential energy wells that enable the cytometer. DEP has been used for many years to manipulate cells for both separations[26−28] and trapping.[29−33] Researchers have succeeded in forming DEP-based particle traps for both micrometer-sized particles, such as cells[29−31] and submicrometer particles, such as virus particles.[32,33] Although it is relatively straightforward to construct a DEP-based particle trap, it is currently difficult to design traps meeting specific quantitative characteristics—in our case, holding of cells against defined fluid flows in addition to being easily arrayable and electrically addressable. However, our cytometer *demands* a trap that meets certain quantitative characteristics, and we have thus used our previously described modeling tools[34] to meet these requirements.

Using these DEP-based particle traps, we have constructed a proof-of-concept realization of the μDAC and demonstrated loading, observation, and arbitrary sorting of cells after collecting their fluorescent dynamic response to a stimulus. Such sorting based upon temporal response uses optical interrogation as a basis for investigating change in cells to an applied stimulus, where the observed change provides a measure of cellular function.

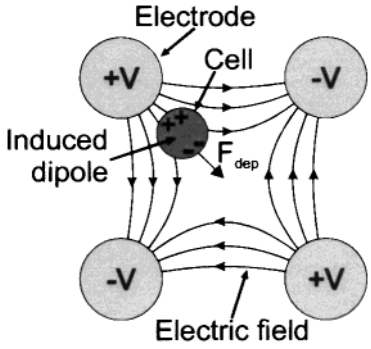

Figure 1. Schematic representation of a quadrupole DEP trap, showing the four electrodes of the quadrupole and a cell trapped in the middle. The n-DEP configuration shown induces an effective dipole moment in the cell that is antiparallel to the electric field. This creates a dielectrophoretic force (F_{dep}) that repels the cell from the electric field, causing it to be stably trapped at the quadrupole's field minimum.

THEORY

Dielectrophoresis (DEP) refers to the force on induced polarization or charge dipoles in a nonuniform electric field.[24,25,31] Essentially, when an electric dipole (or quadrupole, octopole, etc.) is placed in a spatially nonuniform electric field, the Coulombic forces pulling on each end of the dipole are not equal in magnitude (as they would be in a uniform electric field), leading to a net force on the dipole. For DEP-based cell traps, this cellular dipole is induced by the electric field itself. When the induced dipole resides in a medium with some conductivity and permittivity (e.g., a cell in saline), competition between induced polarization in the cell versus the medium determines whether the overall effective dipole moment aligns parallel or antiparallel to the electric field and, thus, whether the DEP force will draw the particle to the field maximum (positive DEP or p-DEP) or minimum (negative DEP or n-DEP), respectively. When the cell is less polarizable than the medium, the effective dipole moment causes n-DEP to occur, and the cell can be stably trapped.[35] (Figure 1).

Due to the fact that the DEP force depends on the field gradient, rather than its direction, one can create net forces with sinusoidally time-varying (AC) fields, which can reduce interactions between the electric fields and the cells, as explained below. In highly conductive aqueous media (e.g., PBS, DMEM, etc.), the cell will be less polarizable than the medium at all frequencies, because both the medium's conductivity and its permittivity will be higher than the cells'. Although operation in such a highly conductive medium could dissipate a significant amount of power, leading to considerable heating, operating at the microscale increases the heat removal rate while decreasing the heat generation volume, limiting temperature excursions. This thus allows us to assay cells in appropriately buffered and supplemented media.

Using high-frequency AC fields (>100s kHz) has several advantages for DEP-based cellular traps. First, operating at such frequencies eliminates any electrophoretic movement of the cell due to its charged membrane. Second, such operation eliminates electrochemical reactions at the electrode−electrolyte interfaces, preventing electrode corrosion and gas formation. Finally, and

(22) Giuliano, K. A.; DeBiasio, R. L.; Dunlay, R. T.; Gough, A.; Volosky, J. M.; Zock, J.; Pavlakis, G. N.; Taylor, D. L. *J. Biomol. Screening* **1997**, *2*, 249−259.
(23) Fu, A. Y.; Spence, C.; Scherer, A.; Arnold, F. H.; Quake, S. R. *Nat. Biotechnol.* **1999**, *17*, 1109−1111.
(24) Jones, T. B. *Electromechanics of particles*; Cambridge University Press: Cambridge, 1995.
(25) Pohl, H. A. *Dielectrophoresis: the behavior of neutral matter in nonuniform electric fields*; Cambridge University Press: Cambridge, 1978.
(26) Huang, Y.; Wang, X.-B.; Becker, F. F.; Gascoyne, P. R. C. *Biophys. J.* **1997**, *73*, 1118−1129.
(27) Cheng, J.; Sheldon, E. L.; Wu, L.; Heller, M. J.; O'Connell, J. P. *Anal. Chem.* **1998**, *70*, 2321−2326.
(28) Talary, M. S.; Mills, K. I.; Hoy, T.; Burnett, A. K.; Pethig, R. *Med. Biol. Eng. Comput.* **1995**, *33*, 235−237.
(29) Fuhr, G.; Arnold, W. M.; Hagedorn, R.; Muller, T.; Benecke, W.; Wagner, B.; Zimmermann, U. *Biochim. Biophys. Acta* **1992**, *1108*, 215−223.
(30) Fiedler, S.; Shirley, S. G.; Schnelle, T.; Fuhr, G. *Anal. Chem.* **1998**, *70*, 1909−1915.
(31) Schnelle, T.; Hagedorn, R.; Fuhr, G.; Fiedler, S.; Muller, T. *Biochim. Biophys. Acta* **1993**, *1157*, 127−140.
(32) Morgan, H.; Hughes, M. P.; Green, N. G. *Biophys. J.* **1999**, *77*, 516−525.
(33) Hughes, M. P.; Morgan, H. *J. Phys. D: Appl. Phys.* **1998**, *31*, 2205−2210.
(34) Voldman, J.; Braff, R. A.; Toner, M.; Gray, M. L.; Schmidt, M. A. *Biophys. J.* **2001**, *80*, 531−541.
(35) Jones, T. B.; Bliss, G. W. *J. Appl. Phys.* **1977**, *48*, 1412−1417.

most importantly, using an external field frequency above the characteristic frequency determined by interfacial charging at the cell membrane can minimize the alternating voltage imposed upon the resting (static) transmembrane voltage.[36] Since electric field-mediated effects are thought to act through imposed transmembrane voltages, high-frequency operation in conjunction with proper biological controls can mitigate such effects.[37−39]

Although the dipole approximation is usually an adequate representation of the DEP force, it does not represent the situation at field nulls, where the induced dipole vanishes, or in fields with high spatial variations, which are common at the microscale. In this case, one must include higher-order multipoles, especially the induced quadrupole, to properly model the traps.[34,40,41] In particular, quadrupole DEP traps, like the one described in this report, trap particles at field nulls, and it is thus necessary to include the induced quadrupole to model them correctly. In our designs, we use our previously developed modeling environment,[34] which can calculate arbitrary induced multipoles, to perform our force modeling.

DEP trapping should be contrasted with electrophoretic manipulation: one cannot stably trap charges in an electrostatic field, whereas it is possible to stably trap induced dipoles.[35] Instead of DEP forces, one might imagine using optical tweezer arrays[42] or microrobot actuators,[43] but those do not combine the capacity for parallelization, simplicity, and holding strength (i.e., confining ability) of DEP traps.

EXPERIMENTAL SECTION

Microfabrication. Microfabrication was as described.[44] Briefly, Ti/Au bilayer thin-film electrodes were evaporated and patterned on glass wafers to form the substrate interconnects. A 60-μm-thick SU-8 photoresist mold then was deposited and patterned, and the cylindrical gold electrodes were electroplated into this mold. The mold was stripped, and then a second 150-μm SU-8 layer was deposited and patterned to form the flow chamber. Fluid access holes were drilled in the chip, and then the chip was capped with a coverslip to complete the device. The final chamber dimensions were 2-mm wide $\times$ 8-mm long $\times$ 150-μm high.

Packaging. Electrical, optical, and fluidic access to the chip was provided using the packaging scheme shown in Figure 2. The chip was connected to a ceramic carrier with double-sided tape. Electrical interconnections were made by wire-bonding from the edge of the microfabricated chip to the ceramic carrier, which sat in a ZIF socket. The ZIF socket was connected to a printed circuit (PC) board that housed the drive circuits. Fluidic connections were made via the flow path shown in Figure 2; the flow was brought via PEEK tubing to an aluminum shunt that sat in a cutout in the ZIF socket. The ceramic carrier mated with the aluminum shunt via O-rings. Ensuring that the complete package had a low profile and that the objectives only had to look thru the coverslip provided optical access compatible with high N. A. fluorescence objectives.

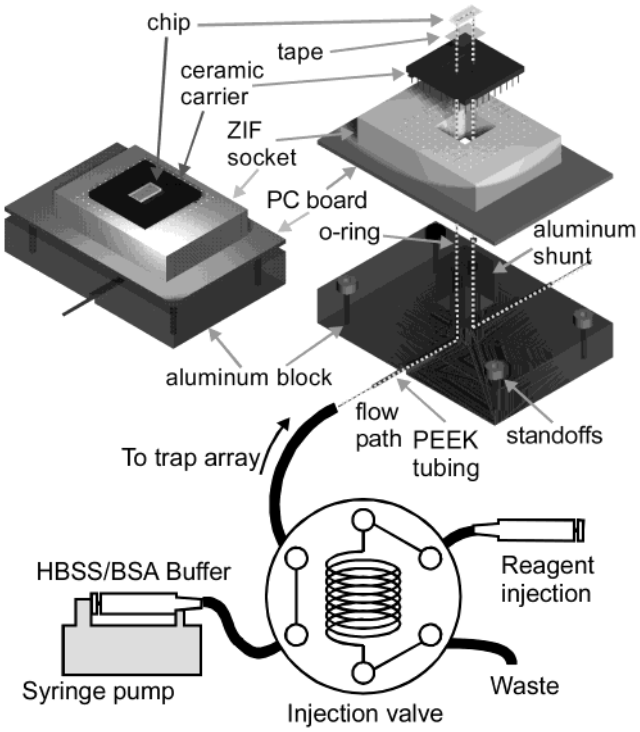

Figure 2. Packaging and test setup. Shown is the fluidic setup used to introduce cells and reagents into the chamber as well as an exploded and unexploded schematic representation of the package itself. The flow is driven by a syringe pump and uses an injection valve to introduce cells and reagents into the flow path. The flow path then proceeds to the package, where it is routed onto and off the chip.

Cells. HL-60 cells were maintained in RPMI 1640 supplemented with 20% fetal bovine serum, 1% L-glutamine and 1% PenStrep. Immediately prior to assay, cell aliquots were washed 3 times and resuspended in Hank's buffered salt solution (HBSS) with 1% bovine serum albumin (BSA), which had a conductivity of 1 S/m. Labeling was performed by incubating for 30 min with calcein-AM (Molecular Probes, Oregon).

Cell Assays. The complete flow path, including the trapping array, was filled and purged before use with HBSS/1% BSA for ~20 min. Cell aliquots in HBSS/1% BSA, with or without calcein labeling, were then introduced into the chamber via the injection valve (Figure 2). Cell capture (Figure 4A), sorting (Figure 5), and dynamic (Figure 6) assays were performed with the electrodes energized with 3 V at 20 MHz and a flow rate of 10 μL/min, whereas the flow was increased to 12 μL/min for the single-cell discrimination assay (Figure 4B). Cell holding experiments (Figure 4C) were performed on 10 random unlabeled HL-60 cells, varying the voltage from 1 to 3 V, the frequency from 1 to 20 MHz, and measuring the release flowrate. Following use, the chamber was purged with HBSS/1% BSA followed by HBSS/0.1% Triton X-100, then DI H_2O, and finally, dried with N_2.

Microscopy. Arrays were imaged using a Zeiss Universal upright microscope equipped with epifluorescence and brightfield

(36) Grosse, C.; Schwan, H. P. T. A. *Biophys. J.* **1992**, *63*, 1632−1642.
(37) Archer, S.; Li, T. T.; Evans, A. T.; Britland, S. T.; Morgan, H. *Biochem. Biophys. Res. Commun.* **1999**, *257*, 687−698.
(38) Wang, X. J.; Yang, J.; Gascoyne, P. R. C. *Biochim. Biophys. Acta* **1999**, *1426*, 53−68.
(39) Fuhr, G.; Glasser, H.; Muller, T.; Schnelle, T. *Biochim. Biophys. Acta* **1994**, *1201*, 353−360.
(40) Hartley, L. F.; Kaler, K.; Paul, R. *J. Electrost.* **1999**, *46*, 233−246.
(41) Washizu, M.; Jones, T. B.; Kaler, K. V. I. S. *Biochim. Biophys. Acta* **1993**, *1158*, 40−46.
(42) Dufresne, E. R.; Grier, D. G. *Rev. Sci. Instrum.* **1998**, *69*, 1974−1977.
(43) Jager, E. W. H.; Inganas, O.; Lundstrom, I. *Science* **2000**, *288*, 2335−2338.
(44) Voldman, J.; Toner, M.; Gray, M. L.; Schmidt, M. A. *Transducers '01*, Munich, Germany, 2001.

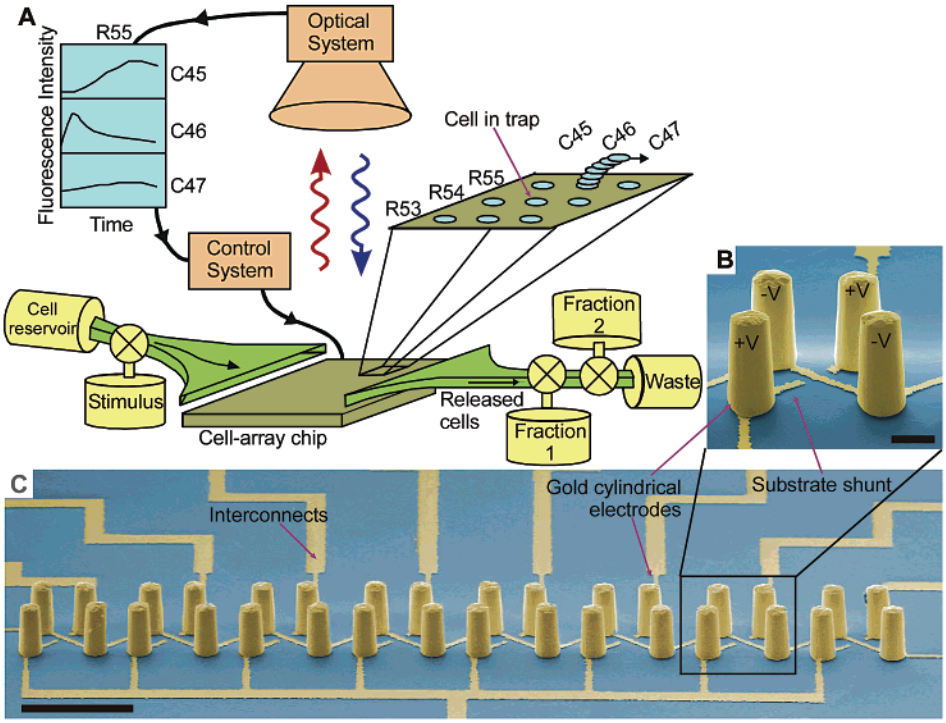

Figure 3. Cytometer overview. (A) Schematic representation of the μDAC, showing single cells loaded onto the cell-array chip and one cell, in row 55, column 46, being sorted by the control system into the fraction collectors after acquisition of dynamic luminescence information from the entire array. (B) Pseudocolored scanning electron micrograph (SEM) showing a single trap consisting of four electroplated gold electrodes arranged trapezoidally along with the substrate interconnects. (C) SEM of a completed 1 $\times$ 8 trap array. Scale bars: (B) 20 μm, (C) 100 μm.

illumination and both a monochrome video camera (Pulnix America, Inc., Sunnyvale, CA) and cooled color CCD camera (Diagnostic Instruments, Sterling Heights, MI). Images were adjusted with Adobe Photoshop for visualization purposes. Post locations were digitally superimposed onto fluorescent images for Figures 4 and 6 to ease visualization.

Trap Modeling. Modeling was performed as described.[34] Predictions for the holding of HL-60 cells in these traps encompassed variations in the trap post diameter (18.5- and 19.0-μm diameters at the top of the posts, with a 3.5-μm taper along its 50-μm length), across the range of cell recorded diameters (9.3−14.4 μm), and across the measured frequency space (1−20 MHz). We used the previously determined electrical properties of HL-60 cells in our calculations.[26] Parameters extracted from the models, such as the electric field and release flowrate, were used to determine the imposed alternating membrane voltage and fluid shear stresses, respectively, to which the cells were exposed. Holding forces were extracted by recording the drag force on the particle at the release flowrate.

RESULTS AND DISCUSSION

A schematic representation of the μDAC is shown in Figure 3A. It consists of three parts: the cell-array chip, where the cells are trapped; an optical system to luminescently interrogate the cells; and a control system that implements the sorting function. In operation, cells from a cell reservoir are flowed onto the cell-array chip and captured by the cell array. A stimulus is then introduced via the fluidic system, after which the integrated optical system interrogates the chip and records luminescence information from each cell. The user, with the help of the control system, decides which cells to release and turns off their respective traps. The released cells flow away from the chip and are sorted and collected by fraction collectors. Here, the cell in row 55, column 46 displays a dynamic response correlated to altered biological function and is released from the cell array and collected for further study (e.g., cloning up, expression analysis, etc.).

The enabling technology for realizing the μDAC is the development of an addressable trap that can be (1) arrayed on a substrate, (2) quickly turned on and off, and (3) can provide strong confinement against fluid flow. The trap should be noncontact, to prevent attachment of cells that would inhibit subsequent release. In addition, the ability to place these traps in a regular array eases the constraints on the optical system, removing the need to locate the cells, as would be the case with cells randomly distributed on a substrate.

To implement our proof-of-concept μDAC, we designed an array of DEP traps using our previously described modeling tools.[34,45] These modeling tools enable us to quantitatively design traps meeting certain requirements, such as strong holding of cells against flow, which in our case we define as being able to hold cells against a flow sufficient to introduce reagents into the chamber in <120 s. Given our final geometry and test setup void volumes, this leads to a need to withstand flows of 12 μL/min, which corresponds to a drag on the cells of ~50 pN. As we have previously shown,[34] planar quadrupoles are inadequate for providing such levels of holding. In addition, each trap in the array is addressable and exhibits strong holding against flow, thus enabling the μDAC.

We fabricated small arrays of these traps as a proof-of-principle vehicle to allow us to demonstrate the distinguishing features of

(45) Voldman, J.; Toner, M.; Gray, M. L.; Schmidt, M. A. *J. Electrost.*, submitted.

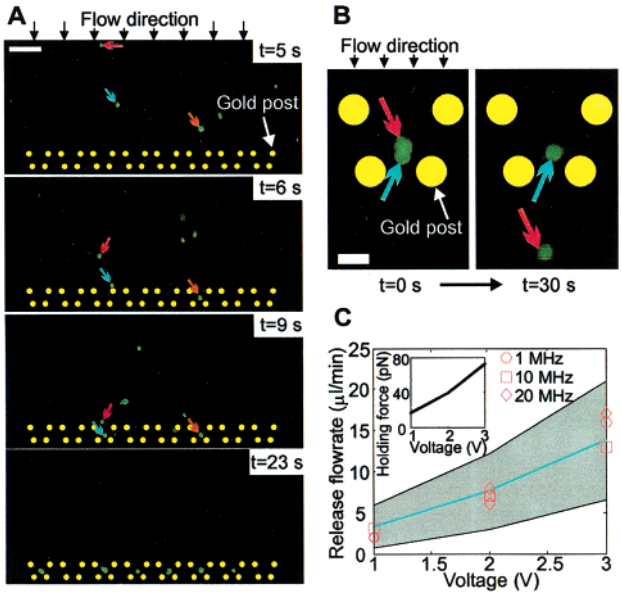

Figure 4. Cell capture. (A) Loading an array of traps with calcein-labeled HL-60 cells. Shown are fluorescence images extracted from video with the post locations superimposed and denoted by yellow circles. The colored arrows track individual cells over time. The time stamp of the frames (after the initiation of flow) is given at the right of each frame. (B) Single-cell discrimination. Shown are two images in a time sequence extracted from video with the superimposed post locations denoted by yellow circles. The arrows follow a particular cell over time. A second trapped cell (red arrow) is stochastically ejected from a trap by applying a higher flowrate than during trap loading, leaving only one trapped cell (green arrow). (C) Cell holding against flow. Results of cell-holding experiments at various frequencies overlaid with a patch (light gray) denoting the bounds on the simulated holding. The inset shows the extracted holding forces obtained using the midline fit (blue line). Scale bar: (A) 100 μm, (B) 20 μm.

the μDAC: noncontact trapping of multiple single cells followed by observation of fluorescent dynamics and subsequent arbitrary sorting.[44] Each trap in the array, shown in Figure 3B,C, consists of four cylindrical gold electrodes that are 20 μm in diameter and 50 μm high. We used this extruded quadrupole structure because it can confine particles over 100 times more strongly (as measured by holding against flow) than a planar quadrupole geometry, yet it allows the flow-chamber height and trap geometry to scale independently (as opposed to planar octopoles).[45] This latter characteristic allows us to maximize holding while minimizing imposed shear stresses and also significantly eases packaging.[45] The posts are arranged trapezoidally and are excited as an electric quadrupole. The asymmetrical trapezoidal arrangement of the posts is used to increase the trapping efficiency, because it lowers the potential energy barrier to loading the trap without affecting the trap strength.[45] On the substrate are gold interconnects that provide electrical excitation and enable the individual traps to be addressed, as well as substrate shunts that enhance trap symmetry to increase trap strength.[45] This trap geometry thus represents significant changes to previously reported DEP-based particle traps, changes which are crucial to realizing the μDAC.

We can load the cytometer by introducing HL-60 cells into the chamber and applying electrical excitation to the electrodes. Figure 4A (and Supporting Information) shows a typical result using a loading density of $\sim 4 \times 10^5$ cells/mL and a flowrate of 10 μL/min. We first introduce cells into the chamber, let them settle for $\sim$1−2 min, and then turn on the flow again to bring the cells to the trapping array. Five seconds after initiating flow, three cells (Figure 4A, arrows) approach the array. At 6 s, one cell (Figure 4A, orange arrow) has been trapped, and a second cell (Figure 4A, blue arrow) is being diverted into another trap. After 9 s, the second cell (Figure 4A, blue arrow) has been trapped, and a third cell (Figure 4A, red arrow) approaches the same trap. Finally, after 23 s, six traps contain at least one cell, and several contain more than 1 cell, demonstrating that under these conditions, we can passively load cells into the trap arrays within 25 s. Qualitative observations indicate that the vast majority of incoming cells that are below the height of the electrodes (50 μm) enter the traps (see Supporting Information).

Once we have successfully loaded the array, we then enforce the requirement that each trap contain only one cell. Since we have not yet implemented closed-loop electrical sensing to ensure single-cell trap loading, we use fluid flow to perform a discrimination step after loading more than 1 cell/trap. By slightly increasing the flow rate from 10 to 12 μL/min, we can distort the potential energy well comprising the trap so that only one cell can be held; any additional cells are ejected from the trap (Figure 4B, and Supporting Information). Essentially, the interaction between the DEP confining forces and the extracting hydrodynamic drag force determines whether cells can be held in the traps. With no flow applied, the trap can hold many particles, limited by the number that can sterically fit within it. At very high flow rates, the drag force will overwhelm the DEP forces, and no particles will be held. There exists an intermediate regime in which one particle, but not two, will "fit" in the trap. In this regime, a second trapped cell is displaced far enough from the potential energy minimum that it ventures outside the potential well and is ejected. In this example, the ejection is stochastic, with a mean lifetime of $\sim$30 s. This lifetime decreases with increasing flowrate.

Central to the operation of the μDAC is loading of the traps followed by the introduction of the fluid reagents. This requires traps that can hold the loaded cells against incoming flows delivering the reagents. The traps need to be strong enough to allow a sufficient flow such that timely introduction of reagents is possible, in our case within 120 s. We thus designed our electrode traps to provide strong confinement against flow while minimizing perturbation of the cell's resting transmembrane voltage. To experimentally demonstrate the holding strength, we can vary the voltage applied to the electrodes and measure the ability of the traps to hold cells by determining the minimum flow under which the cells are liberated, the release flowrate. This gives a measure of the strength of the traps and, thus, their suitability for use in our cytometer. Our models can then be used to extract the imposed perturbations to the cell's resting transmembrane voltage, giving an indication of possible electric field-cell interactions.

We performed measurements on 10 random unlabeled HL-60 cells in HBSS, varying the voltage from 1 to 3 V, the frequency from 1 to 20 MHz, and measuring the release flowrate. The results indicate that HL-60 cells can be held in these traps under flows of about 12−15 μL/min at 3 V (Figure 4C). Comparing the measured holding to experimental predictions, we see that the predictions span a space demarked by the variations in fabricated trap geometry, measured cell diameters, and applied frequencies

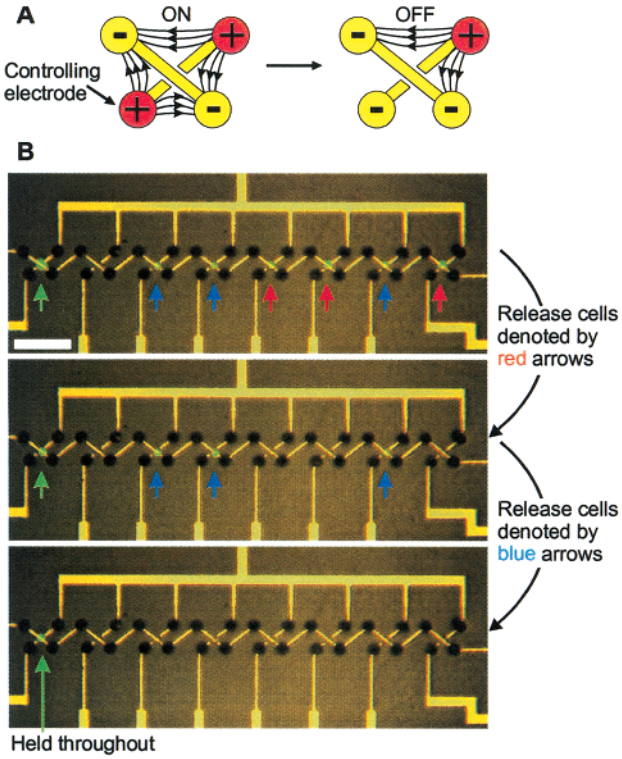

Figure 5. Cell sorting. (A) Schematic representation of operation. Switching the potential on the controlling electrode from $+V$ to $-V$ disrupts the quadrupolar potential energy well by removing the electric field cage (compare to Figure 3), thus ejecting the cell. (B) Series of composite brightfield and fluorescence images illustrating selective and independent trap control. HL-60 cells are individually released in a defined yet arbitrary manner. We first sorted all the cells in traps designated by the red arrows and then all the cells in traps designated by the blue arrows, leaving only a single activated trap (green arrow). Scale bar: 100 μm.

(Figure 4C, gray patch). Using an approximate best fit to the data (Figure 4C, blue line), we can get approximations for inferred quantities. For example, the calculated holding forces for our traps are ~70 pN at 3 V and are monotonically dependent on the applied voltage (Figure 4C, inset); these forces are equal to or greater than those obtained with optical tweezers.[46,47] In addition, the calculated approximate fluid shear on the cells is 0.03 Pa at 12 μL/min, smaller than would be expected to induce cellular responses (data not shown).

From the validated model we can extract the transmembrane voltage that we impose across the cells. We extract from the model the electric field at the cell's location in the trap at release, and using standard electric models of the cell[36] and the cell's electrical parameters, we can calculate the imposed transmembrane voltage. At 3 V and 20 MHz, the field produces a synchronous (20 MHz) alternating transmembrane voltage on HL-60 cells of 12 mV, which is 20 times smaller than it would be at DC. This thus shows the efficacy of operating at high frequency.

We can address the traps in the array by controlling the potential of one electrode in each trap. Switching this potential from $+V$ to ground disrupts the confining field cage and, thus, ejects the particle (Figure 5A). Using this arrangement, we can

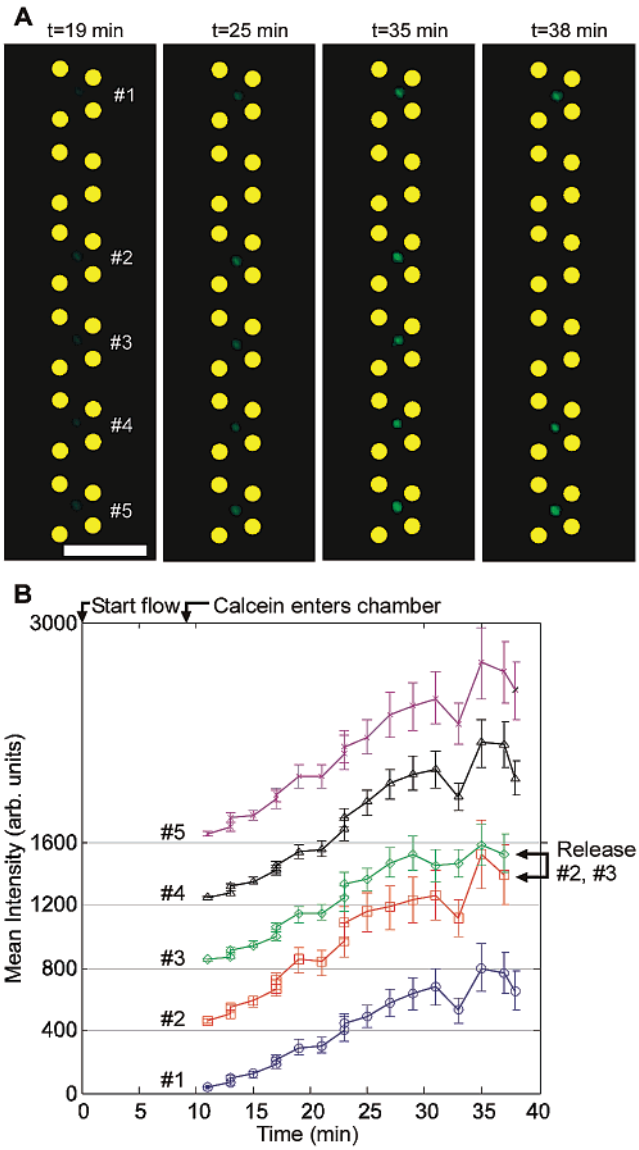

Figure 6. Dynamic calcein-loading assay followed by sorting. (A) Time sequence of fluorescence images of HL-60 cells being loaded with 10-μM calcein in HBSS. (B) Extracted fluorescence intensity profiles for the five sites shown in (A), averaged over the cell area. The mean intensities from each trap are offset by 400 intensity units for clearer display. Also indicated are the timepoints at which flow was initiated and cells entered the chamber. Subsequent microscopy indicated that two cells were present in traps 2, 3, and 5. Scale bar: 100 μm.

arbitrarily sort cell populations (Figure 5B). Here, we have loaded the array with seven calcein-labeled HL-60 cells. By switching the individual traps, we can controllably and repeatedly release directed subpopulations of cells into the flow. This, coupled with the ability to observe trapped cells over time, enables us to interrogate and then viably sort cell subpopulations.

We used calcein-loading of HL-60 cells as a surrogate assay to demonstrate observation of luminescent dynamics in an array of cells with single-cell resolution followed by sorting. We introduced unlabeled HL-60 cells in HBSS into the chamber and loaded them into the array. We then switched our fluid stream to introduce 10-μM calcein in HBSS into the chamber. As the calcein entered the chamber, it was loaded into the cells, causing their fluores-

(46) Svoboda, K.; Block, S. M. *Ann. Rev. Biophys. Biomol. Struct.* **1994**, *23*, 247−285.
(47) Ashkin, A. *Proc. Natl. Acad. Sci. U.S.A.* **1997**, *94*, 4853−4860.

cence to increase over time (Figure 6). We recorded fluorescence images from the entire array every two minutes for 38 min. The concentration of calcein used caused the cellular fluorescence of the trapped cells to become visible ~2 min after entry into the chamber and with similar dynamic responses across the array. At the end of the experiment, we switched off two of the traps to release their cells and thus effect sorting.

These studies demonstrate the ability to obtain luminescence information from multiple traps over many minutes and *then* sort. Thus, one can obtain the full dynamic response of a population of cells and *then* decide what the sort parameter should be and implement the sorting function. It also points to several engineering challenges for the next generation of devices. Careful observation noted that several of the traps in the array contained two cells, not one. Thus, the operating conditions chosen were not stringent enough to impose single-cell discrimination for these pairs of cells, which can be addressed with a closed-loop electrical sensing scheme to ensure that traps are loaded with only one cell.

The μDAC is well-poised for application to large-scale single-cell manipulation. Although engineering challenges remain in scaling up, operating, and imaging a large array of traps, no fundamental problems exist. Besides the dynamic assays described herein, this array cytometer has several other potential uses. First, because the μDAC can potentially image cells prior to sorting, it could enable the isolation of cell populations on the basis of intracellular information (e.g., separating cells based upon nuclear localization dynamics). Second, the arrayed and individually addressable nature of the traps could enable one to investigate phenotypic differences across different cell lines by spatially multiplexing different cell lines in different traps and exposing them all to the same stimulus. Finally, since the cells are held at defined locations from the substrate, one could perform shear studies on suspended objects (e.g., to investigate shear-induced gene expression in leukocytes).

ACKNOWLEDGMENT

This work was supported in part by the Alliance for Cellular Signaling (NIGMS #1U54GM62114-01) and by the Edward Hood Taplin Professorship (M.L.G.). J.V. was supported by consecutive NSF and Kodak graduate research fellowships. We thank Stephen D. Senturia, Alfred G. Gilman, and James C. Weaver for their comments on the manuscript. We also thank the Microsystems Technology Laboratories at MIT for fabrication assistance and Ann Black for help with cell culture.

NOTE ADDED AFTER ASAP POSTING

This article was inadvertently posted ASAP before a correction was made to the caption for Figure 3. The corrected version was posted with the issue.

SUPPORTING INFORMATION AVAILABLE

A listing (2 Quicktime movies showing loading of the array with HL-60 cells and single-cell discrimination) is available as Supporting Information. This material is available free of charge via the Internet at http://pubs.acs.org.

Received for review March 11, 2002. Accepted May 24, 2002.

AC0256235